Astron. Astrophys. 332, 325–338 (1998)

ASTRONOMY
AND
ASTROPHYSICS

A statistical approach to the investigation of fine structure of solar prominences

S. Pojoga[1,3], **A.G. Nikoghossian**[2,3], **and Z. Mouradian**[3]

[1] Astronomical Institute of Romanian Academy, RO-75212 Bucharest, Romania
[2] Byurakan Astrophysical Observatory, 378433 Byurakan, Armenia
[3] Observatoire de Paris-Meudon, DASOP, F-92195 Meudon Cedex, France

Received 21 October 1997 / Accepted 11 December 1997

Abstract. A statistical approach is proposed for the study of the prominence fine structure in EUV lines ($T = 10^4$ to 3×10^5 K). For different regions of several solar prominences, the distributions of the observed intensities, and their averaged characteristics (mean intensity and relative variance) are determined. We develop a statistical model, assuming that the observed intensities and their fluctuations are generated by a random number of fine-structure elements along the line-of-sight. Different models are considered, for the lines formed in the cool plasma and in the hot transition zone. For the structural components, two geometries – slabs and threads – are assumed. We compare the statistical characteristics of the intensity, inferred from theoretical models, with those obtained from observations. The influence of the geometrical model on the degree of the brightness variations is analysed. The expected number of fine-structure components along the line-of-sight is also derived. We show that, generally, the geometry is not of major importance for the study of the spatial brightness fluctuations. A relative small mean number of fine-structure elements along the line-of-sight is determined.

Key words: Sun: prominences – Sun: transition region – radiative transfer

1. Introduction

Solar prominences consist of a number of fine-structure elements such as threads, knots, blobs, etc. (Engvold 1976, Tandberg-Hanssen 1995). The dimensions of these components vary throughout the prominence, and the smallest are generally supposed to be less than the spatial resolution of the instrument (Tandberg-Hanssen 1995). One of the main problems of solar prominences is to determine the geometry and the physical properties of the fine structure, which is difficult, sometimes impossible, to establish directly by observations, because of the small sizes of the elements and their superposition along the line-of-sight. In order to estimate the emitting volume, several authors consider the observed pixel to be partially occupied by the prominence material and use the concept of the filling factor without any reference to the geometry of the structural elements (Engvold et al. 1987). The filling factor is defined as the ratio between the emitting surface and the area encompassed by a pixel of the instrument. A more realistic approach should consider an explicit form for the geometry and the number of sub-resolution structures. Attempts to determine the role of the geometrical factors were made by Orrall & Schmahl (1980) who studied the emission and absorption of solar prominences in the HI Lyman continuum for two geometrical models: resolved slabs and unresolved cylindrical threads. They found slightly different estimates for the total optical thickness and the number of structural elements in the line-of-sight, the lower limit ranging from 4 to 10, depending on the model. Several other methods also have been employed to determine the number of the sub-resolution structures along the line-of-sight. Engvold et al. (1989), analysing the CaII, K line profiles, derived a number of thread-like elements within one arcsec^2, of about $3 - 5$. Applying a model of random clustering of components to observations of Hα spectra, Zirker & Koutchmy (1990) found the average number of threads within one arcsec^2 to be 16 in bright regions and 7 in faint regions of the prominence.

The present paper suggests a somewhat different approach, based on a statistical investigation of the spatial and temporal variations of the prominence brightness. We start assuming that the intensity fluctuations are due to the random character of the geometrical and physical properties of the structural elements. Hence, when observing certain distributions of the intensity over the set of pixels, we are concerned with an ensemble of various realisations of these characteristics. The theoretical determination of the intensity observed within each pixel is equivalent to the solution of a certain deterministic problem of radiative transfer. Having this solution, one may construct the theoretical distribution of intensity and compare it to that obtained from observations thus providing additional information on the geometrical and physical parameters of prominences. The extreme

Send offprint requests to: S. Pojoga

ultraviolet (EUV) spectra of prominences represent a rich observational material suitable for a statistical treatment.

The spatial brightness variations of prominences may have several reasons: differences in the line-of-sight number of structural elements and in the value of the filling factor, physical inhomogeneities of the structures, instrumental errors and so on. These factors must be studied separately in order to determine the significance of each in establishing the variations. An idealised model problem accounting for the random distribution of the internal energy sources in the prominence was treated by Nikoghossian et al. (1997). In the present work, we assume that the statistical fluctuations of the emerging intensity are due exclusively to the random number of components along the line-of-sight. Following Orrall & Schmahl (1980), two geometrical models are adopted for the structural elements: slabs (1D) and cylindrical threads (2D).

In Sect. 2 we describe the prominence observations, as well as the statistical method. The theoretical models and the averaged characteristics of the distributions are presented in Sect. 3. Different assumptions are considered for the region of line formation: emission occurring in the cool parts of the prominences (Sect. 3.1) and in the transition region (Sect. 3.2). Sect. 4 analyses the statistical characteristics of the intensity for different geometries. The observed intensity distributions and their statistical features as well as their comparison with the theoretical predictions are described in Sect. 5. In Sect. 5.3 we derive the expected number of structures in the line-of-sight. A brief summary and the principal conclusions are given in Sect. 6.

2. Observations

Our observations were obtained by the Harvard College Observatory spectrometer on ATM aboard Skylab (Reeves et al. 1977). In the raster mode, the instrument produced simultaneous spectroheliograms in seven wavelengths in the EUV spectral range. Images were obtained during 5.5 minutes with 5×5 arcsec^2 spatial resolution over a field of view of 5×5 arcmin^2.

The range of wavelengths includes emission lines and continua formed at temperatures between 10^4 and 10^6 K. Along with the HI Lyman series lines that contain information about the cool parts of the prominences at approximately 10^4 K, the observed EUV spectrum includes emission lines of ionic species formed in the prominence-corona interface and lower corona. We distinguish between the optically thin lines CII λ1336Å, CIII λ977Å and OVI λ1032Å ($\lambda > 912$ Å), and the lines OIV λ554Å and MgX λ625Å which exhibit strong absorption in the Lyman continuum. Using simultaneous observations in these lines we achieve information about the plasma at several temperatures and, consequently, about various structures or different regions of the same structure of the prominence.

The observations are summarised in Table 1. Meudon Observatory H-α spectroheliograms were available and were used for positioning.

2.1. The statistical treatment of observational data

The statistical treatment of the images studies the distributions of intensities for all spectral lines. The averaged characteristics of these distributions we used are: the mean intensity, $\langle I \rangle$, and the relative mean square deviation (RelMSD or relative variance),

$$\delta = \frac{\langle I^2 \rangle}{\langle I \rangle^2} - 1. \quad (1)$$

To have reliable statistics, we selected prominences with a large number of observed pixels and with long time series. From each prominence we chose relatively quiet regions, physically different and situated at various heights above the limb. The regions were required to be relatively homogeneous so that the brightness variations could be considered to be random, rather than being due to changes in the morphology of the prominence. These regions were also required to be large enough, to provide a sufficiently wide volume of statistics. This latter, rather stringent requirement, was difficult to satisfy by every prominence. In some cases, this difficulty was overcome by the use of subsequent images of the same prominence taken during a time interval of 10–20 minutes. This procedure was justified by a preliminary statistical analysis which revealed that, generally, the temporal intensity variations of these prominences during such time intervals were probably random and not due to changes in the physical conditions or structure.

The observed distributions and the statistical parameters were generally found to vary depending on the position of the prominence region (height above the limb or distance from the footpoint). The results of the statistical analysis are presented in Sect. 5.

2.2. Instrumental noise

We shall first consider the role of instrumental noise and scattered light on the measurements. For this study, we need observations of a stable and uniform emission in the same range as for the observed prominences. In this sense, our data are poor and offer little information. Quiet sun areas exhibit important changes 5.5 minutes, which are likely to be of solar origin (Vernazza et al. 1975). Some information is given by Reeves et al. (1977) who present the results of the tests and calibration of the instrument. Their conclusion was that the detectors used had a very low background noise and that "under constant illumination the detection system produces a nearly constant count rate and operated on a stable counting plateau". They also mentioned that in the telescope, the level of scattered light from the solar disk beyond 2.5" from the edge of the slit was less than 1% in one pixel and had no time or density dependence. The scattered light in the spectrometer for detector 1 was 1.2 counts/sec which gives a noise/signal ratio of about 2×10^{-3} for CIII and 5.5×10^{-3} for Ly-α in the range of prominence intensities. There was no evidence of any modulation of the expected photon distribution by the instrument.

Table 1. Solar prominences observed by HCO spectrometer and used in this study.

No.	Date 1973	Position	Number of images	UT	Observed lines and wavelengths (Å)
1	July 10	$-31°$E	8	21:45–22:24	CII 1336, Ly-α 1216, OVI 1032, CIII 977, Ly-C 896, MgX 625, OIV 554
2	Aug 30	-31°W	1	14:02	CII 1336, Ly-α 1216, OVI 1032, CIII 977, Ly-C 896, MgX 625, OIV 554
3	Aug 30	-27°W	3	14:53–15:03	Ly-α 1216, Ly-β 1026, Ly-γ 972, Ly-C 890
4	Aug 30	-27°W	1	20:09	CII 1336, Ly-α 1216, OVI 1032, CIII 977, Ly-C 896, MgX 625, OIV 554
5	Aug 30	-29°W	1	21:24	CII 1336, Ly-α 1216, OVI 1032, CIII 977, Ly-C 896, MgX 625, OIV 554
6	Dec 18	39°E	1	0:00	Ly-α 1216, Ly-β 1026, Ly-γ 972
7	Dec 18	30°E	9	8:47–9:31	CII 1336, Ly-α 1216, OVI 1032, CIII 977, MgX 625, OIV 554
8	Dec 18	25°E	1	14:10	CII 1336, Ly-α 1216, OVI 1032, CIII 977, MgX 625, OIV 554
9	Dec 18	25°E	2	16:38–16:42	Ly-α 1216, Ly-β 1026

For some "empty" sky regions, we calculated the mean values of the noise intensities. These areas were situated at a relatively large distance from the limb and only lines formed at low temperatures were considered. Therefore, we assumed that the observed features did not belong to the corona, but were instrumental noise and scattered light. The following values were found for the noise/prominence intensity ratio: 2.5×10^{-3} for CII, 1.6×10^{-3} for CIII and 1×10^{-3} for Ly-α. We consider these quantities too small to be taken into account.

All these facts permit us to assume that the measured fluctuations in prominences are of solar origin and that the instrumental noise is negligible, to an inferior limit of $\sim 2\%$ of the local intensity.

2.3. Effect of the coronal background

The influence of the surrounding corona on the measured values of intensity is important only for lines of highly ionised atoms at temperatures approaching coronal values. In our study, this concerns especially the OVI λ1032Å line, which has a significant contribution of coronal background. The line MgX λ625Å was not considered, as it forms at higher temperatures and provides less information, if any, about prominences. Our interest in this line concerns only its absorption in the cool parts of the prominence. The knowledge of $\langle I_{\rm cor}\rangle$, $\delta_{\rm cor}$ for corona and $\langle I_{\rm p+c}\rangle$, $\delta_{\rm p+c}$ for prominence plus coronal background, makes it possible to evaluate the similar values for the prominence alone. These quantities are related according to the formulas

$$\langle I_{\rm p+c}\rangle = \langle I_{\rm pr}\rangle + \langle I_{\rm cor}\rangle\,, \tag{2}$$

$$\delta_{\rm p+c} = \frac{\langle I_{\rm pr}\rangle^2\,\delta_{\rm pr} + \langle I_{\rm cor}\rangle^2\,\delta_{\rm cor}}{\left(\langle I_{\rm pr}\rangle + \langle I_{\rm cor}\rangle\right)^2}, \tag{3}$$

Table 2. Values of mean intensity, $\langle I\rangle$, and RelMSD, δ, in the OVI 1032 line for prominence with coronal background (p+c), corona (cor) and prominence (pr) at several heights above the limb (observations from December 18, 1973).

height	$\langle I\rangle$(counts)			δ		
(arcsec)	p+c	cor	pr	p+c	cor	pr
47.5	45.36	14.0	31.36	0.152	0.135	0.292
52.5	42.30	12.0	30.30	0.137	0.155	0.243
60.0	31.36	10.5	20.86	0.067	0.160	0.112
70.0	24.81	9.2	15.61	0.080	0.165	0.146
72.5	22.45	9.0	13.45	0.118	0.165	0.255
85.0	26.56	7.0	19.56	0.073	0.170	0.113

where the last is an alternative representation of the summation law for standard deviations: $\sigma^2_{\rm p+c} = \sigma^2_{\rm pr} + \sigma^2_{\rm cor}$.

The values of $\langle I_{\rm cor}\rangle$ and $\delta_{\rm cor}$, at different heights above the limb, were inferred from images of the quiet corona. Because of the inhomogeneous nature of the solar corona, the averaged structures and the volume of the coronal material differ from those in the presence of a prominence. Hence, the values of $\langle I_{\rm cor}\rangle$ and $\delta_{\rm cor}$, estimated for the pure corona, only approximately describe the corona surrounding a prominence. Table 2 presents the values of the mean intensity and RelMSD inferred from the prominence and corona observations of 1973 December 18, and the deduced values of these quantities for the prominence alone. As might be expected, the RelMSD for the corona shows a small increase with height above the limb. We see that, in accordance with the summation law for the standard deviations, the quantity $\delta_{\rm p+c}$ is less than those for the prominence ($\delta_{\rm pr}$) and corona ($\delta_{\rm cor}$) alone, at the same heights above the limb. Thus, the overlapping corona smoothes out the real

brightness variations of the prominence. This effect is more pronounced when the mean intensities of the coronal background become comparable with those of the prominence alone. In our further analysis we use the values of $\langle I_{\rm pr} \rangle$ and $\delta_{\rm pr}$ obtained after substracting the contribution of the corona.

3. Theoretical models

As mentioned above, both the physical and geometrical characteristics of the fine-structure elements may be regarded as being random, thus causing fluctuations in the brightness of prominences. The influence of variations in the physical conditions of the fine structures on the observed intensities was recently discussed by Nikoghossian et al. (1997). We consider now the effect of the geometrical factors, such as the shape of these components and their number along the line-of-sight.

A model's fine structure consists of a cool region (10^4 K) having a simple geometry (1D or 2D, see below) and a transition region to the hot corona. Considering the transfer of radiation through such randomly distributed entities, we investigate the statistical properties of the emerging intensities and compare them to those obtained from observations. In order to derive the theoretical intensity distributions as well as the analytical expressions for the mean intensity and RelMSD we make the following assumptions:

- The fluctuations of the observed intensities are due only to the random character of the number of fine structures in the line-of-sight.
- These components have identical dimensions, structure and physical properties. This is a rough approximation to consider for the whole prominence. We presume that the above properties are identical in the studied prominence areas, but might change when passing from one region to another.
- The line-of-sight number of elements is distributed according to Poisson's law. The choice of the Poisson distribution seems reasonable, especially in describing the intensity variations in rarefied regions of prominences.

Our observations allow us to consider several layers of the prominence-corona atmosphere, from the cool prominence to the hot coronal plasma. Hence, we consider two cases for the line-formation regions. The first assumes that the line forms in the cool core of the structure, which is more or less optically thick, so that the radiated energy is partially absorbed within the core. The absorption through the envelope and corona is neglected. We refer to this case as "core emission". It can be applied to the study of the lines of hydrogen Lyman series as well as to the Lyman continuum ($\lambda < 912$ Å). In the second case, the region of line formation is the transition zone of the features. This interface is considered to be optically thin, and the radiation may be absorbed only in the core region. This case will be referred as "interface emission". It can be used to treat lines like OIV λ554Å, CII λ1336Å, CIII λ977Å and OVI λ1032Å. The temperature of the core region is roughly 15–20,000 K.

Finally, we consider two geometrical models for the fine-structure elements that we average within the volume encompassed by a pixel.

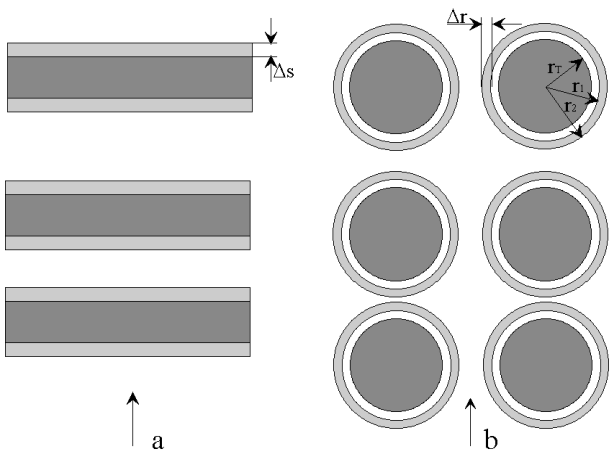

Fig. 1a and b. The geometrical models considered for fine structure elements of prominence: **a** slab model (N = 3), **b** thread model (N = 3, M = 2)

The first geometrical model (1D) supposes a homogenous prominence region to be made up of a finite and randomly distributed number of slabs of cool material separated by inter-slab coronal plasma (see Fig. 1a). Each slab shows a transition zone between the core and corona. The slabs completely cover the pixel area and the number of slabs in the line-of-sight may vary from one pixel to another. This case approximates complex structures when their dimensions normal to the line-of-sight are larger than the instrumental resolution.

The second model (2D) assumes that the observed volume is filled with a finite number of cylindrical threads embedded in the hot coronal material, each of them containing cool plasma, surrounded by a transition zone (see Fig. 1b). They are supposed to be identical and parallel to one axis of the pixel. The diameter of the threads is much smaller than the linear pixel dimension, whereas their length greatly exceeds it. For simplicity, we consider that the threads are arranged one behind another in the line-of-sight and that each pixel embraces several such rows of an equal number of threads.

The analytical expressions for the observed pixel intensity, mean intensity and RelMSD of the line radiation were derived for the models presented above.

3.1. The core emission

We begin with considering the core emission that concerns lines emitted and absorbed in the central cool part of the structures.

3.1.1. Slab geometry

Suppose that we have a prominence region containing n slabs along the line-of-sight (see Fig. 1a). In a given spectral line, the intensity coming from the k-th feature is

$$i_k = S_k \left(1 - \mathrm{e}^{-\tau_k}\right), \tag{4}$$

where τ_k is the optical thickness and S_k the source function of the core. We consider these quantities to be constant within the

slab and the same for all slabs and denote them, τ and S. After absorption through the $k-1$ components situated in front of the k-th slab, the contribution of this to the total intensity becomes

$$I_k = S\left(1-\mathrm{e}^{-\tau}\right)\mathrm{e}^{-(k-1)\tau}. \tag{5}$$

Consequently, the intensity from the set of n slabs is given by the sum of all these contributions

$$I(n) = \sum_{k=1}^{n} I_k = S\left(1-\mathrm{e}^{-n\tau}\right). \tag{6}$$

Let us suppose now that, in a given prominence area, the number of structures in the line-of-sight is distributed according to Poisson's law $p(n) = N^n\mathrm{e}^{-N}/n!$, where $N = \sum_{n=0}^{\infty} np(n)$ is the Poisson mean of n. Hence, the mean intensity from this prominence region is (Fig. 2a,b)

$$\langle I\rangle = \sum_{n=0}^{\infty} p(n)\, I(n) = S\left(1-\mathrm{e}^{-Nq(\tau)}\right), \tag{7}$$

where $q(\tau) = 1-\mathrm{e}^{-\tau}$. Accordingly, the RelMSD defined by Eq. (1) is (Fig. 3a,b)

$$\delta = \mathrm{e}^{-2Nq(\tau)}\frac{\mathrm{e}^{Nq(\tau)^2}-1}{\left(1-\mathrm{e}^{-Nq(\tau)}\right)^2}. \tag{8}$$

Note that in the optically thick case ($\tau \gg 1$) we have $q = 1$ and the mean intensity and RelMSD do not depend on τ and are given by

$$\langle I\rangle = S\left(1-\mathrm{e}^{-N}\right); \quad \delta = \frac{1}{\mathrm{e}^N-1}, \tag{9}$$

If also $N \gg 1$, we obtain

$$\langle I\rangle = S; \quad \delta = 0. \tag{10}$$

When deriving Eqs. (7) and (8), the effects of multiple scattering were ignored, and this is inadmissible for strong opaque lines such as the lines of the HI Lyman series. Consideration of the scattering process makes the problem of finding $\langle I\rangle$ and δ too complicated to be given here. Even so, the problem admits essential simplification for the pure scattering case. This special situation is of primary importance in considering the Ly-α line in prominences. Since now all the energy released in the medium escapes, we have $I(n) = nS\tau$ so that

$$\langle I\rangle = NS\tau; \quad \delta = \frac{1}{N}. \tag{11}$$

Note that for $N\tau \ll 1$, i.e., when the medium is transparent, Eqs. (7) and (8) transform into Eqs. (11). This is not surprising, since in this limiting case, again, all the emitted energy escapes the medium.

3.1.2. Thread geometry

Consider now a cylindrical element and let r_T be the radius of the core, S_T the core source function, and τ_T the total optical thickness along the core diameter (Fig. 1b). The intensity of radiation coming from a slice situated at the distance x (in units of r_T) from the thread centre is

$$I(x) = S_\mathrm{T}\left(1-\mathrm{e}^{-\tau_\mathrm{T}\sqrt{1-x^2}}\right). \tag{12}$$

Consequently, for the energy radiated by a 1 cm high thread one finds

$$E = 2S_\mathrm{T}r_\mathrm{T}\int_0^1\left(1-\mathrm{e}^{-\tau_\mathrm{T}\sqrt{1-x^2}}\right)\mathrm{d}x. \tag{13}$$

The intensity given by a row containing n identical elements arranged one behind another in the line-of-sight is

$$I(n) = S_\mathrm{T}\int_0^1\left(1-\mathrm{e}^{-n\tau_\mathrm{T}\sqrt{1-x^2}}\right)\mathrm{d}x. \tag{14}$$

In general, the volume observed within one pixel may include several such rows and then the equation of intensity for a pixel contains a term depending on the number and distribution of the rows, equivalent to a filling factor. Hence, if we consider that a pixel contains a number of M rows of threads, the observed intensity must be multiplied by $\gamma = \frac{2r_\mathrm{T}M}{l}$, where l is the aperture of the spectrometer.

A Poisson distributed number of threads, leads to the mean intensity and the RelMSD (Figs. 2a,b and 3a,b)

$$\langle I\rangle = S_\mathrm{T}\gamma\left(1-\int_0^1\mathrm{e}^{-Np(\tau,x)}\mathrm{d}x\right) \tag{15}$$

$$\delta = \frac{\int_0^1\int_0^1\mathrm{e}^{-N[p(\tau,x)+p(\tau,y)]}\left[\mathrm{e}^{Np(\tau,x)p(\tau,y)}-1\right]\mathrm{d}x\mathrm{d}y}{\left(1-\int_0^1\mathrm{e}^{-Np(\tau,x)}\mathrm{d}x\right)^2}, \tag{16}$$

where $p(\tau,x) = 1-\mathrm{e}^{-\tau_\mathrm{T}\sqrt{1-x^2}}$. If $\tau \gg 1$, we are led to Eqs. (9), and if also $N \gg 1$, to Eqs. (10), as for the slab model, the mean intensity involving in this case the factor γ.

It should be emphasised that a reasoning similar to that in the foregoing section, leads for pure scattering to the following formulas (here we are able to adopt a more realistic assumption that the total number Mn of threads within a pixel is a random quantity being subject to Poisson's law)

$$\langle I\rangle = \frac{\varepsilon VK}{l^2}; \quad \delta = \frac{1}{K}, \tag{17}$$

where $K = \langle Mn\rangle$, and $V = \pi r_\mathrm{T}^2 l$ is the volume of a thread. Note that Eqs. (17) are valid for any arrangement of threads in space.

3.2. The interface emission

Let us treat now the second approach, applicable to lines emitted in the interface and absorbed in the core.

3.2.1. Slab geometry

In the slab geometry, each structure is plane-parallel and has a central absorbing layer and two emitting envelopes for which absorption is neglected. The radiation emerging from the interface opposite to us with respect to the core is absorbed in passing trough the core and adds to the radiation emerging from the interface toward us. The observed intensity emerging from a set of n such structures arranged one behind another along the line-of-sight is

$$I(n) = \varepsilon \Delta s \left(1 - \mathrm{e}^{-n\tau} + 2\sum_{k=1}^{n} \mathrm{e}^{-k\tau}\right), \tag{18}$$

where $\varepsilon, \Delta s$ are the line emissivity and the geometrical thickness of each interface, respectively; τ is the optical thickness of the core. Performing the summation in Eq. (18) we may write

$$I(n) = \varepsilon \Delta s \left[\frac{1+\mathrm{e}^{-\tau}}{1-\mathrm{e}^{-\tau}}\left(1-\mathrm{e}^{-n\tau}\right)\right]. \tag{19}$$

Assuming a Poisson distribution of n, we obtain for the mean intensity and the RelMSD of a given region (Figs. 4a,b and 5a,b)

$$\langle I\rangle = \varepsilon \Delta s \left[\frac{2-q(\tau)}{q(\tau)}\left(1-\mathrm{e}^{-Nq(\tau)}\right)\right], \tag{20}$$

$$\delta = \mathrm{e}^{-2Nq(\tau)} \frac{\mathrm{e}^{Nq(\tau)^2}-1}{\left(1-\mathrm{e}^{-Nq(\tau)}\right)^2}, \tag{21}$$

where, as above, $q(\tau) = 1 - \mathrm{e}^{-\tau}$. In the limiting case of an optically thin central layer ($\tau \ll 1$), we have $q = \tau$ and the above quantities become

$$\langle I\rangle = \frac{2\varepsilon\Delta s}{\tau}\left[\left(1-\mathrm{e}^{-N\tau}\right)\right], \tag{22}$$

$$\delta = \mathrm{e}^{-2N\tau} \frac{N\tau^2}{\left(1-\mathrm{e}^{-N\tau}\right)^2}, \tag{23}$$

or, if $N\tau \ll 1$,

$$\langle I\rangle = 2N\varepsilon\Delta s, \tag{24}$$

$$\delta = \frac{1}{N}. \tag{25}$$

In the opposite extreme case, when $\tau \gg 1$ and also $N \gg 1$, we arrive again at Eqs. (9) and (10), as for core emission, with S replaced by $\varepsilon\Delta s$.

3.2.2. Thread geometry

Finally, we derive the theoretical expression for the intensity for the thread geometrical model, considering an approach similar to that of Orrall & Schmahl (1980). We assume that a structure presents a cylindrical absorbing core with radius r_T surrounded by an optically thin emitting shell. In general, this interface is supposed to be separated from the core and lies between r_1 and r_2 ($r_\mathrm{T} \le r_1 \le r_2$). As in Sect. 3.1.2 we may write the energy radiated by a 1 cm high thread

$$E = 2\int_{r_1}^{r_2} \varepsilon r \mathrm{d}r \int_0^{\pi/2} \left(1+\mathrm{e}^{-\tau_\mathrm{T}\sqrt{1-x^2}}\right)\mathrm{d}\varphi, \tag{26}$$

where φ is the angular coordinate in cylindrical geometry and τ_T, the optical thickness along the core diameter.

As pointed out by several authors (Engvold et al. 1987, Tandberg-Hanssen 1995), the geometrical thickness of the interface is presumed to be very small compared with the thread's diameter. As a consequence, for most of the lines formed in the interface, r_1 and r_2, which delimit the region of line formation, are very close to r_T. Hence, it is of particular interest to consider the limiting case of a infinitely thin interface, with $r_1 = r_2 = r_\mathrm{T}$. This simpler problem enables one to write down less complex expressions for the emerging intensity. Considering isotropic emission, we introduce the quantity ε_s which characterises the energy radiated by unit square of an infinitely thin wall of the cylindrical thread. Thus, $\varepsilon = \varepsilon_\mathrm{s}\delta(r - r_\mathrm{T})$ and Eq. (26) takes the form

$$E = 2\varepsilon_\mathrm{s} r_\mathrm{T} \int_0^1 \left(1+\mathrm{e}^{-\tau_\mathrm{T}\sqrt{1-x^2}}\right)\frac{\mathrm{d}x}{\sqrt{1-x^2}}. \tag{27}$$

If we consider a row formed by n threads, this quantity becomes

$$E(n) = \int_0^1 \frac{1+2\sum_{k=1}^{n} \mathrm{e}^{-k\tau_\mathrm{T}\sqrt{1-x^2}} - \mathrm{e}^{-n\tau_\mathrm{T}\sqrt{1-x^2}}}{\sqrt{1-x^2}}\mathrm{d}x \times 2\varepsilon_\mathrm{s} r_\mathrm{T}, \tag{28}$$

and, after performing the summation, the intensity in one pixel is given by

$$I(n) = \gamma\varepsilon_\mathrm{s} \int_0^1 \frac{(2-p(\tau,x))\left(1-\mathrm{e}^{-n\tau_\mathrm{T}\sqrt{1-x^2}}\right)}{p(\tau,x)\sqrt{1-x^2}}\mathrm{d}x, \tag{29}$$

where $p(\tau,x) = 1 - \mathrm{e}^{-\tau_\mathrm{T}\sqrt{1-x^2}}$, the parameter γ being defined in Sect. 3.1.2.

For the Poisson distribution for the number of threads, the mean intensity and the RelMSD are (Figs. 4a,b and 5a,b)

$$\langle I\rangle = \gamma\varepsilon_\mathrm{s} \int_0^1 \frac{2-p(\tau,x)}{p(\tau,x)}\left[1-\mathrm{e}^{-Np(\tau,x)}\right]\frac{\mathrm{d}x}{\sqrt{1-x^2}}, \tag{30}$$

$$\delta = \frac{(\gamma\varepsilon_\mathrm{s})^2}{\langle I\rangle^2}\int_0^1\int_0^1 A_1(\tau,x)\,\mathrm{e}^{-Np(\tau,x)} \times A_1(\tau,y)\,\mathrm{e}^{-Np(\tau,y)}\left[\mathrm{e}^{Np(\tau,x)p(\tau,x)}-1\right]\mathrm{d}x\mathrm{d}y, \tag{31}$$

where $A_1(\tau,x) = \frac{2-p(\tau,x)}{p(\tau,x)\sqrt{1-x^2}}$. Both extreme values of the optical thickness are of interest. If $N\tau \ll 1$, it follows, from Eqs. (30) and (31), that

$$\langle I\rangle = \pi\gamma N\varepsilon_\mathrm{s}; \quad \delta = \frac{1}{N}. \tag{32}$$

When $\tau \gg 1$, and also $N \gg 1$, the mean intensity and RelMSD have the same dependence on N as in the core-emission case, Eqs. (9) and (10), with S substituted by $\frac{\pi}{2}\gamma\varepsilon_{\rm s}$.

Let us now consider the general case of the extended interface. It is customary to pass in what follows to the dimensionless distances scaled by $r_{\rm T}$, and we write $a_1 = r_1/r_{\rm T}$ and $a_2 = r_2/r_{\rm T}$. The energy radiated by a 1 cm high thread, which has an emitting envelope between $r_1$and r_2, and an absorbing core with radius $r_{\rm T}$ is

$$E = 2\varepsilon r_{\rm T}^2 \int_0^1 \omega(x, a_1, a_2)\left(1 + {\rm e}^{-\tau_{\rm T}\sqrt{1-x^2}}\right){\rm d}x + 4\varepsilon r_{\rm T}^2 C(a_1, a_2), \quad (33)$$

where $\omega(x, a_1, a_2) = \sqrt{a_2^2 - x^2} - \sqrt{a_1^2 - x^2}$ and $C(a_1, a_2) = \int_1^{a_2}\sqrt{a_2^2 - x^2}{\rm d}x - \int_1^{a_1}\sqrt{a_1^2 - x^2}{\rm d}x$. For the intensity in one pixel containing n threads in the line-of-sight, we obtain the following expression

$$I(n) = \frac{\gamma\varepsilon r_{\rm T}^2}{r_2}\int_0^1 \frac{1 + {\rm e}^{-\tau_{\rm T}\sqrt{1-x^2}}}{1 - {\rm e}^{-\tau_{\rm T}\sqrt{1-x^2}}}\left(1 - {\rm e}^{-n\tau_{\rm T}\sqrt{1-x^2}}\right)\omega{\rm d}x + \frac{2\gamma n\varepsilon r_{\rm T}^2}{r_2}C(a_1, a_2). \quad (34)$$

We see that the two items in Eq. (34) exhibit different dependences on the number of threads, n. The first is given by the radiation emitted by the envelope, and undergoes absorption in the core, while the second corresponds to the rays coming from the "wings" of the interface, which do not intersect the core. This last component largely depends on the size of the interface. While it is negligible for a tiny interface, it may become important if the envelope is large enough, especially when the number of structures is large. We observe that the intensity in the 2D model depends, besides on the size of the interface, also on the dimension of the thread through the quantity $r_{\rm T}^2/r_2$. We may write $r_{\rm T}^2/r_2 = 4\Delta r_{\rm m}/\pi\left(a_2^2 - a_1^2\right)$, where $\Delta r_{\rm m}$ is an averaged line-of-sight thickness of the cylindrical shell, i.e. the thickness of a slab interface having the same emitting volume as the thread interface. Consequently, when n obeys the Poisson distribution, the mean intensity and RelMSD resulting from Eq. (34) are given by (Figs. 4a,b and 5a,b)

$$\langle I\rangle = \left[\int_0^1 A_2(\tau, x)\left(1 - {\rm e}^{-Np(\tau,x)}\right){\rm d}x + 2NC(a_1, a_2)\right] \times \varepsilon\Delta r_{\rm m}\frac{4\gamma}{\pi\left(a_2^2 - a_1^2\right)}, \quad (35)$$

$$\delta = \frac{1}{\langle I_{\rm a}\rangle^2}\int_0^1\int_0^1 A_2(\tau, x)\,{\rm e}^{-Np(\tau,x)}A_2(\tau, y)\,{\rm e}^{-Np(\tau,y)} \times\left({\rm e}^{Np(\tau,x)p(\tau,y)} - 1\right){\rm d}x{\rm d}y + \frac{4NC^2(a_1, a_2)}{\langle I_{\rm a}\rangle^2} + \frac{4NC(a_1, a_2)}{\langle I_{\rm a}\rangle^2}\int_0^1 A_2(\tau, x)\,p(\tau, x)\,{\rm e}^{-Np(\tau,x)}{\rm d}x, \quad (36)$$

where $A_2(\tau, x) = \frac{2-p(\tau,x)}{p(\tau,x)}\omega(x, a_1, a_2)$ and $\langle I_{\rm a}\rangle$ is the term in brackets in Eq. (35). We see that if the interface is adjacent to the core then $r_1 = r_{\rm T}$, or $a_1 = 1$, and letting $r_2 \to r_{\rm T}$ we arrive at the case of the infinitely thin interface.

In the limiting case when $N\tau \ll 1$, Eqs. (35) and (36) become

$$\langle I\rangle = \frac{\pi}{2}N\varepsilon\gamma\frac{r_2^2 - r_1^2}{r_2} = 2N\varepsilon\gamma\Delta r_{\rm m}; \quad \delta = \frac{1}{N}, \quad (37)$$

and give a behaviour of the two parameters similar to the core-emission case. When $\tau \gg 1$, and also $N \gg 1$ one finds from Eqs. (35) and (36) that

$$\langle I\rangle = \frac{4\varepsilon\gamma\Delta r_{\rm m}}{\pi\left(a_2^2 - a_1^2\right)}\left[C_1(a_1, a_2) + 2NC(a_1, a_2)\right], \quad (38)$$

$$\delta = \frac{4NC^2(a_1, a_2)}{\left[C_1(a_1, a_2) + 2NC(a_1, a_2)\right]^2}, \quad (39)$$

where $C_1(a_1, a_2) = \int_0^1 \omega(x, a_1, a_2)\,{\rm d}x$.

4. Discussion of the theoretical models

We have now covered all the prerequisites for elucidating the role of the geometry of the fine-structure elements in the statistical characteristics of the intensity fluctuations. In this section, we compare the two theoretical models. The functions $\langle I(N, \tau)\rangle$ and $\delta(N, \tau)$ were obtained, assuming arbitrary values for the mean number of structures in the line-of-sight, N, and the optical thickness of the core, τ. Having analytic formulas for the intensity, one may construct the probability distributions of intensity assuming a Poisson distribution of the number of components. The behaviour of these theoretical distributions is also discussed.

When comparing the different models, we note that the explicit expressions for the mean intensity involve some constant factors which are a priori generally unknown. However, their influence is not essential for our purpose, which principally consists in a comparative analysis of various geometrical models. Moreover, it is natural to compare quantities estimated for the same amount of the initial release of energy or absorbing properties of a single structure. Consequently, we use the dimensionless mean intensities, scaled by I_0, where $I_0 = S = \gamma S_{\rm T}$ for core emission and $I_0 = \varepsilon\Delta s = \pi\gamma\varepsilon_{\rm s}/2 = \varepsilon\gamma\Delta r_{\rm m}$ for interface emission. We also take an averaged optical thickness of the cylindrical core, $\tau_{\rm m} = \tau_{\rm T} \times \pi/4$ instead of its maximum value, $\tau_{\rm T}$.

When an extended interface is considered for the thread-like geometry, both the mean intensity and RelMSD further depend on the geometrical thickness and on the location of the emitting layer with respect to the absorbing layer (through the parameters $a_1 = r_1/r_{\rm T}$ and $a_2 = r_2/r_{\rm T}$). Practically, as we specified in Sect. 3.2.2, the size of the interface is very small compared with the diameter of the threads, so that we can assume that a_1 and a_2 take values close to 1 (~ 1.01 or even less). For values in this range, the sensitivity of the $\langle I\rangle$ and δ functions on variations

of these two parameters is very small, except for large τ values (see Figs. 4 and 5). Therefore, we can approximate that a_1 and a_2 are constant when τ is varying.

The behaviour of $\langle I \rangle$ and δ with τ and N, is plotted in Figs. 2a,b and 3a,b for the core-emission model. Figs. 4a,b and 5a,b show the dependence on τ and N of the mean intensity and RelMSD respectively, for envelope emission. The values of N were chosen in such a way that the theoretical values of δ would be in the proximity of the observational values (see Table 3).

4.1. Core emission

We see from Fig. 2a,b that the quantity $\langle I \rangle / I_0$ is a monotonically increasing function of N and τ for both geometrical models. The dependence on the two variables, very strong at low values, is reduced at higher N, and especially at higher τ, values. In fact, at large τ values, we see that the mean intensity depends, for both models, only on N, as also follows from Eq. (9). It is noteworthy that, in the slab model, the mean intensity is always slightly greater than in the thread model. This difference is larger for intermediate values of τ and N and diminishes rapidly when τ increases. From Fig. 3a,b we see that the influence of the geometrical factor is negligible on the RelMSD. The function is decreasing with increasing N and τ, particularly at low values of the two parameters. For $\tau > 2$, for example, δ becomes rather insensitive to τ variations, and tends to 0 with increasing N (see Eqs. 9 and 10).

The geometrical model is not of major importance for the probability distributions of intensity in the core-emission case. The mean intensity value, determined by both N and τ, gives the location of the distribution function on the intensity coordinate axis. The asymmetry is due to the optical thickness and the maximum value to the number of elements. For large τ values the distribution is strongly asymmetrical, tailed to small intensities. As the optical thickness decreases, the distribution changes first to a symmetrical shape and then to an asymmetrical one, tailed to large intensity values (see Fig. 6a).

For the pure scattering case (Eqs. 11 and 17), the mean intensity is also increasing with optical thickness and the mean number of elements, but it is not saturating at great values of these parameters. The RelMSD is determined only by N and has an identical value to that obtained for a transparent medium. Therefore, both geometrical models predict the same decrease of the relative variance with the number of components. It is easy to observe from Eqs. (11) and (17) that in this case the theoretical intensities exhibit a Poisson-like distribution (see Fig. 6a).

The physical interpretation of the results is easy to understand. When the prominence is more transparent, the role of the variation of the number of structures is greater. Consequently, the relative fluctuations are larger and the observed intensity exhibits a distribution that retains the salient traits of the Poisson distribution. For the optically thick lines, this is especially the case of the rarefied regions of the prominence, where the Poisson nature of fluctuations appears to be beyond doubt. With increasing τ, the mean intensity grows larger and is saturating, and the opaque prominence may cause only minor fluctuations of intensity. This is an expected result because if the radiation is received principally from the nearest elements, supposed identical, fluctuations will vanish. Taking also into account the role of N, we find that the greater the total optical thickness in a given line is, the smaller are the values taken by δ. As we shall see later, this relationship may be traced by considering the lines of the HI Lyman series.

We conclude that *the geometrical model of the components is not of major importance for the degree of brightness fluctuations in the core-emission case*. Therefore, when analysing the variations of intensity, a single geometry may be considered.

4.2. Interface emission

The emitting envelope is important for lines formed in the transition region. This model assumes that the radiation may partially be absorbed when propagating through the cores of structures that lie in the line-of-sight. Two extreme cases of the optically thin and thick cores are of particular interest. The first may be applied to the lines CII λ1336Å, CIII λ977Å and OVI λ1032Å, for which the attenuation of radiation in the core is absent or extremely small. The second case can be applied to the lines OIV λ554Å and MgX λ625Å which fall shortward of the Lyman limit and undergo absorption in the Lyman continuum.

The quantity $\langle I \rangle$ is plotted as a function of τ (Fig. 4a) and N (Fig. 4b), considering some different values of the parameters a_1 and a_2 for the extended shell model. For all the geometrical models, the mean intensity is an increasing function of N but, as absorption occurs only in the core, a decreasing function of τ. Like in the core-emission case, this dependence on the two variables diminishes at large τ. We note that the values obtained in the thread model are always higher than those in the slab model. The smallest difference occurs when absorption in the core is weak, in which case the functions – for both slab and thread geometries – tend to $\langle I \rangle = 2N$ (see Fig. 4b). The difference between the $\langle I \rangle$ values accentuates at higher values of τ and N. If the total optical thickness of the medium is large, the mean intensity for the infinitely thin interface model approaches that for the slab model. For $\tau \geq 2$, the latter is almost constant and is given by the nearest emitting envelope ($\varepsilon \Delta s$). When an extended interface is taken into account, the mean intensity is higher and can grow further, if the interface is greater in size or distant from the core.

Fig. 5a,b show the dependence of the RelMSD on τ and N for different values of a_1 and a_2. We see that the function has a similar behaviour with respect to τ and N, as in the core-emission case. Moreover, for the slab model, the RelMSD for interface emission and core emission is given by the same formula (cf. Eqs. 8 and 21). We see that the relative variance in the thread-like case is always greater than in the slab-like case. At low τ values, small differences appear between the models, and all predict the same value, $\delta = 1/N$, at $\tau = 0$. With increasing τ, the split among the δ curves becomes larger. When strong absorption occurs, this difference diminishes between slabs and infinitely thin interface threads, which give $\delta \simeq 0$ for $N \geq 10$.

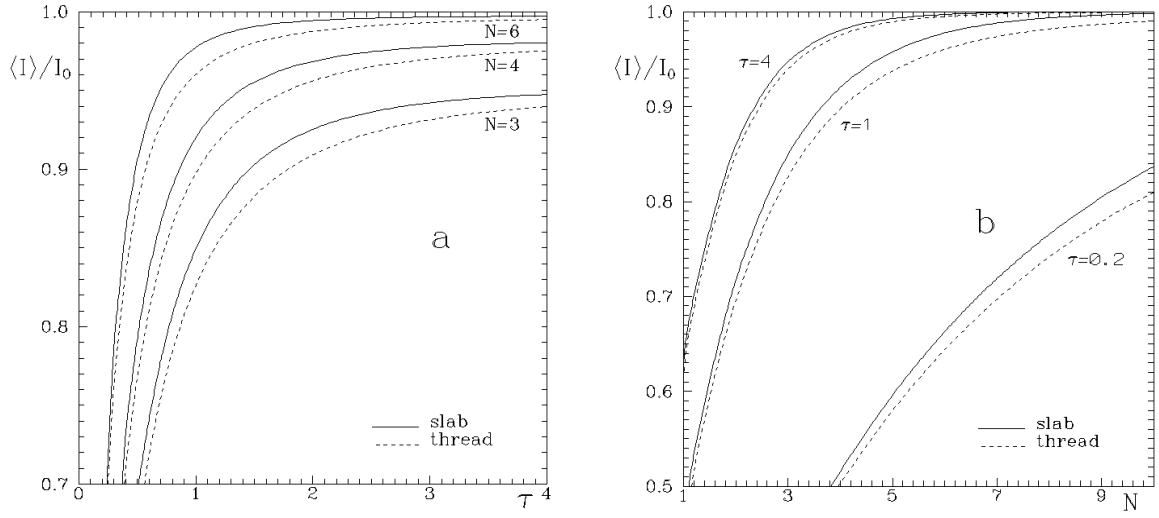

Fig. 2a and b. The theoretical mean intensities, $\langle I(N,\tau)\rangle$, scaled by the initial energy released by a single layer, I_0, deduced from the core-emission model. The dependence upon: **a** the optical thickness of the core, **b** the expected number of structures in the line-of-sight

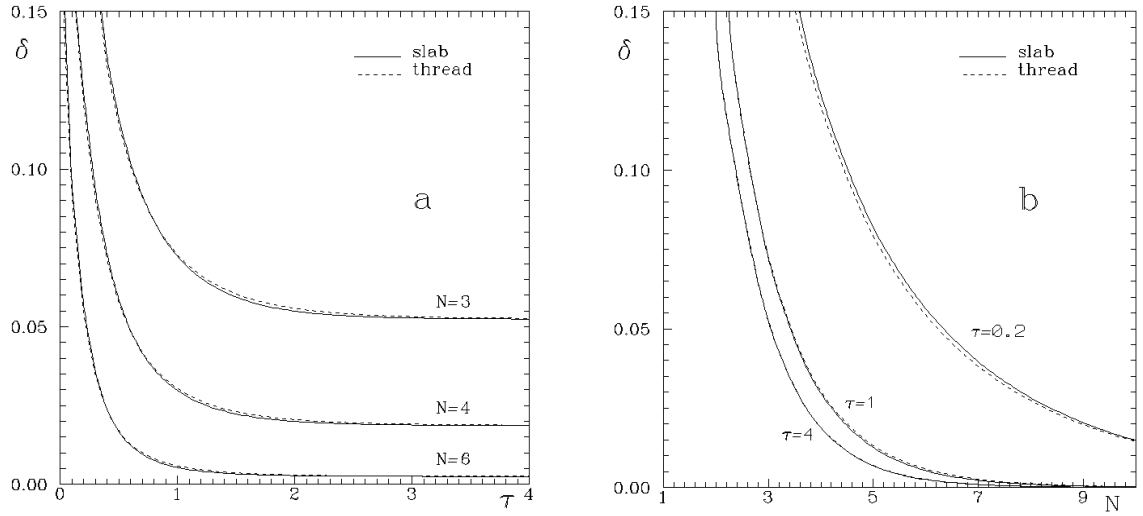

Fig. 3a and b. The theoretical RelMSD, δ, for the core-emission model. The dependence upon: **a** the optical thickness of the core, **b** the expected number of structures in the line-of-sight

The extended envelope model yields greater values of δ and a non-zero limit for $N \to \infty$.

The theoretical probability distributions of the observed intensity exhibit the same dependence on the number of elements, optical thickness, and mean intensity as for the core-emission model. For an optically thin core, the main case of interest, the distributions are always asymmetrical and tailed toward larger intensity values (see Fig. 6b). The geometrical model induces significant differences between the theoretical distributions only for large values of the optical thickness.

Most of the specific features of functions $\delta(N,\tau)$ and $\langle I(N,\tau)\rangle$ in this model, have a physical interpretation analogous to that for the core emission. Generally, an opaque prominence provides saturation of the mean intensities and small fluctuations. In particular, the Poisson nature of the intensity fluctuations becomes essential for an optically thin prominence. We emphasize that, when the optical thickness of the core becomes significant, the extended interface model differs from the slab and the infinitely thin models. In this case, both $\langle I\rangle$ and δ contain an additional term given by the radiation that does not intersect the core, and consequently does not exhibit absorption in the core. Its contribution to the total intensity is not negligible for a large and distant interface. As we shall see in the next section, sometimes the resulting behaviour of this model may be closer to the real situations, when a more complex geometrical structure of the randomly arranged fine elements may lead us to similar results.

In conclusion, we may state that *the role of the geometrical model is not important in determining the values of* $\langle I\rangle$ *and* δ*, when the total optical thickness of the medium is small. How-*

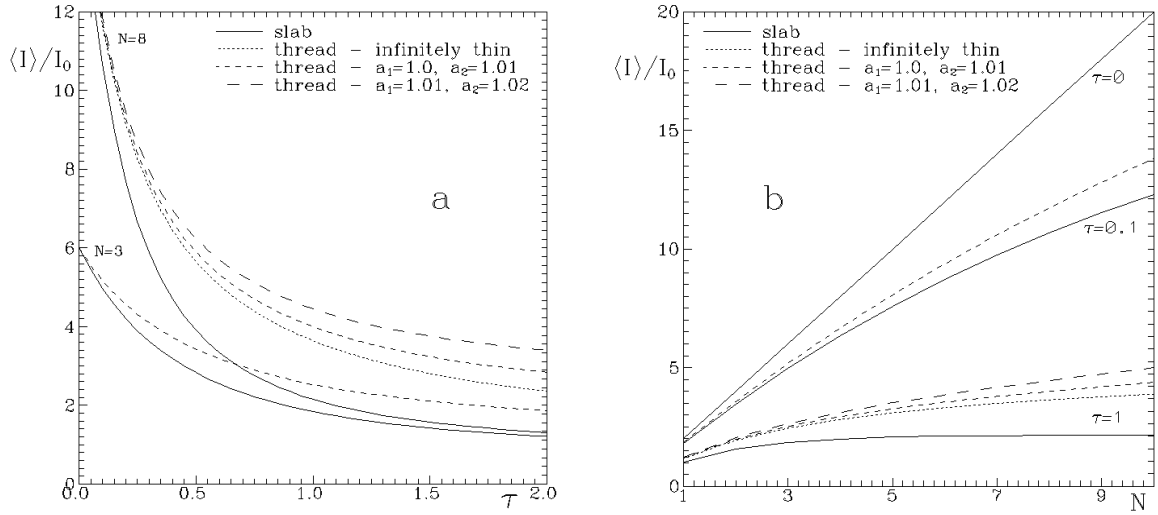

Fig. 4a and b. The theoretical mean intensities, $\langle I(N,\tau)\rangle$, scaled by the initial energy released by a single layer, I_0, for the interface-emission model. The dependence upon: **a** the optical thickness of the core for two values of the mean number of structures (for $N = 3$, only the case $a_1 = 1$, $a_2 = 1.01$ was considered), **b** the expected number of structures in the line-of-sight for three values of the optical thickness of the core (for $\tau = 0.1$, only the case $a_1 = 1$, $a_2 = 1.01$ was considered)

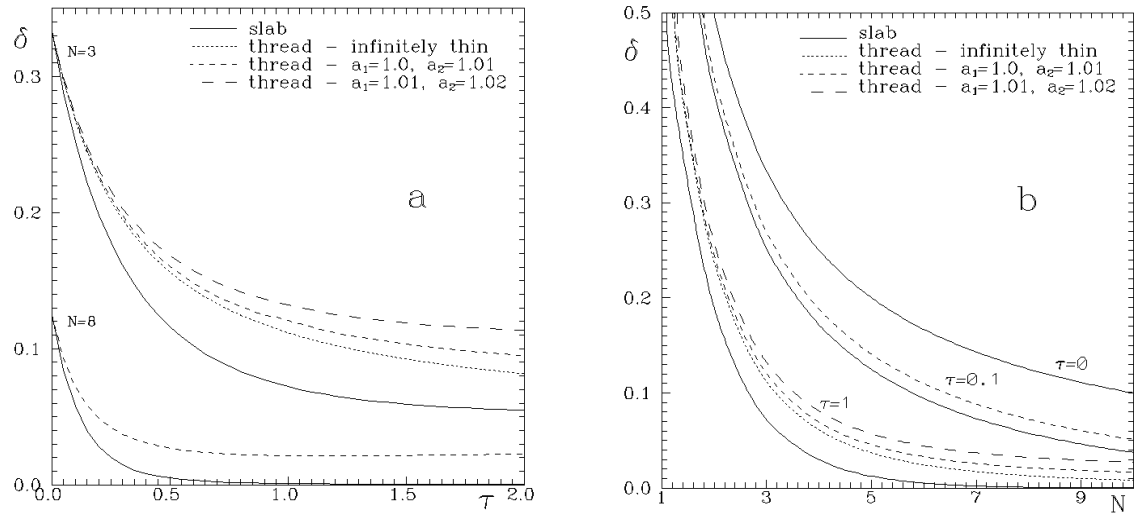

Fig. 5a and b. The theoretical RelMSD, δ, for the interface-emission model. The dependence upon: **a** the optical thickness of the core for two values of the mean number of structures (for $N = 8$, only the case $a_1 = 1$, $a_2 = 1.01$ was considered), **b** the expected number of structures in the line-of-sight for three values of the optical thickness of the core (for $\tau = 0.1$, only the case $a_1 = 1$, $a_2 = 1.01$ was considered)

ever, this influence becomes greater at higher values of N and τ. When the volumes of the emitting and absorbing material are fixed, a given number of opaque threads causes greater fluctuations than the same number of opaque slabs. *For interface emission, the infinitely thin envelope model is a rather good approximation for the thread geometry when the optical thickness of the core is not too elevated.*

5. Observations and models

In this section we present the results of the statistical analysis of observational data, and compare them to the models discussed above. We found that the statistical properties of the emerging radiation show an evident dependence on the magnitude of the observed intensity. Thus, we analyse the relative variance for various prominence regions, using the mean intensity as parameter.

Table 3 gives $\delta_{\rm obs}$ for some typical prominence regions. As compared to our previous studies, involving the statistical characteristics of the observed prominence intensities, a number of other observations were added (see Pojoga et al. 1997). The values of the RelMSD shown in Table 3 represent a synthesis of all the observations employed, that include more than 30 regions from 5 prominences. Concerning the mean intensities, corre-

Table 3. Typical values for the RelMSD, δ, in the observed prominences. Concerning the mean intensities of the studied areas, we may generally find a factor of approximately 1.4 between the bright and normal and also between the normal and faint regions.

Spectral line	Region brightness		
	Bright	Normal	Faint
Ly-α 1216	0.02–0.06	0.04–0.08	0.07–0.2
Ly-β 1026	0.04–0.06	0.06–0.085	0.075–0.1
Ly-γ 972	0.07	0.07–0.1	–
Ly-C 896	0.04–0.05	0.045–0.08	0.07–0.2
CII 1336	0.04–0.2	0.05–0.25	0.1–0.3
OVI 1032	0.015–0.13	0.04–0.1	0.07–0.13
CIII 977	0.01–0.13	0.025–0.1	0.06–0.1
MgX 625	0.1–0.3	0.15–0.3	0.2–0.3
OIV 554	0.1–0.4	0.07–0.5	0.1–0.6

sponding to the values of δ, we find a factor of approximately 1.4 between both the bright and normal and the normal and faint regions.

5.1. Core emission

The core-emission model can be applied to the study of the radiation emitted in the cool parts of the structures, like the lines of the HI Lyman series as well as the Lyman continuum. It predicts small δ values for an optically thick medium for both geometrical models. The decrease of the RelMSD with τ, and with N, presented in Fig. 3a,b can be traced considering the optically thick lines.

For the same prominence region we see from Table 3 that, generally, δ(Ly-α) $<$ δ(Ly-β) $<$ δ(Ly-γ). Therefore, the estimates of the opacity for these lines lead us to the same behaviour as for the theoretical case, i.e. the larger the optical thickness of a structural element in a given spectral line, the smaller the brightness variations. We cannot determine quantitatively the difference between the optical thicknesses because in this limiting case δ is less sensitive to τ. Small values of the RelMSD are also found for the Lyman continuum intensities.

On the other hand, supposing that the more intense regions contain a greater number of structures and assuming a constant optical thickness of the elements, the predicted decrease of δ with the mean number of elements is also observed. For the optically thick lines, we see from Table 3 that, considering successively brighter regions of the prominence, we generally find smaller fluctuations. This behaviour of the fluctuations was also detected by Stellmacher & Wiehr (1994), from observations in the Hα and Hβ lines, and can be treated within the framework of the core-emission model. We note that, when passing from one observed area to another, the optical thickness may also change, due to the variation of the structures' density. Therefore, the decrease of the RelMSD in the bright regions can also be given by the increase of τ. In conclusion, the behaviour of the observed values of δ follows the theoretical decrease with increasing N and τ, given by the core-emission approach. Note that the pure scattering mechanism also predicts a decrease of the relative variance with the number of elements (see Eqs. 11 and 17) outlined above.

Let us examine the distributions of the observed intensities over magnitudes. For the optically thick lines, the observations show a Gaussian-like probability distribution. An observed Ly-α distribution together with the theoretical distributions, for different values of the mean number of structures, are shown in Fig. 6a. For a quantitative evaluation of the Gaussian representation, we used Kolmogorov's λ-criterium (Stuart & Ord 1991). Assuming the observed values of $\langle I \rangle$ and δ as parameters for the Gaussian, we achieve an agreement with the observational distribution with 90–99% confidence. Nevertheless, we see from Fig. 6a that the core-emission model leads to an asymmetrical theoretical distribution tailed to smaller intensities, which differs from a Gaussian to a large extent. The curves were obtained using the pairs (N, τ) given by the observed values of δ. If N increases, and τ decreases, the theoretical distribution fits observations better. Hence, for the core-emission model, a good agreement with the observed distributions is obtained only for low values of the optical thickness of a structure, which are not suitable for the Ly-α and the Ly-β lines. On the other hand, supposing pure scattering as the basic mechanism responsible for the Ly-α formation, we obtain a Poisson-like distribution of intensities. For an increase of the Poisson parameter (in our case the mean number of structures) the Poisson distribution tends to a Gaussian and differs only slightly from the latter. This fact occurs even for relatively not very large values of this parameter, bringing nearer the theoretical and observational distributions. Such an example is illustrated in Fig. 6a.

5.2. Interface emission

The interface model is used for lines emitted in the hotter regions of the prominence features. We first consider the optically thin lines which might undergo a very small absorption if any, in the cool parts. As illustrated in Table 3 , the optically thin lines (CII λ1336Å, CIII λ977Å, OVI λ1032Å) exhibit somewhat higher relative fluctuations. This is an expected result, since the model indeed predicts that the intensity variations for an optically thin medium are greater than in the case of absorption. Particularly, if $\tau \to 0$ all geometrical models yield $\delta \to 1/N$. Assuming that the brightest regions are characterised by the largest N values, the behaviour of the observational values of δ for the OVI and CIII lines is, in general, in agreement with the theoretical expectation i.e., the greater the mean intensity, the smaller the relative variance. This is illustrated in Fig. 7 that gives the dependence of the RelMSD on the mean intensity. The points represent the values for the CIII and OVI lines, calculated from images of 9 different regions of a prominence, observed on July 10, 1973. The curve represents the theoretical expectation given by Eqs. (24) and (25). However, some departures from this behaviour occur for some of the other prominences, where the RelMSD is slightly higher for the brightest areas (see Table 2). This could be due to the failure of Poisson's law in dense regions, or to the

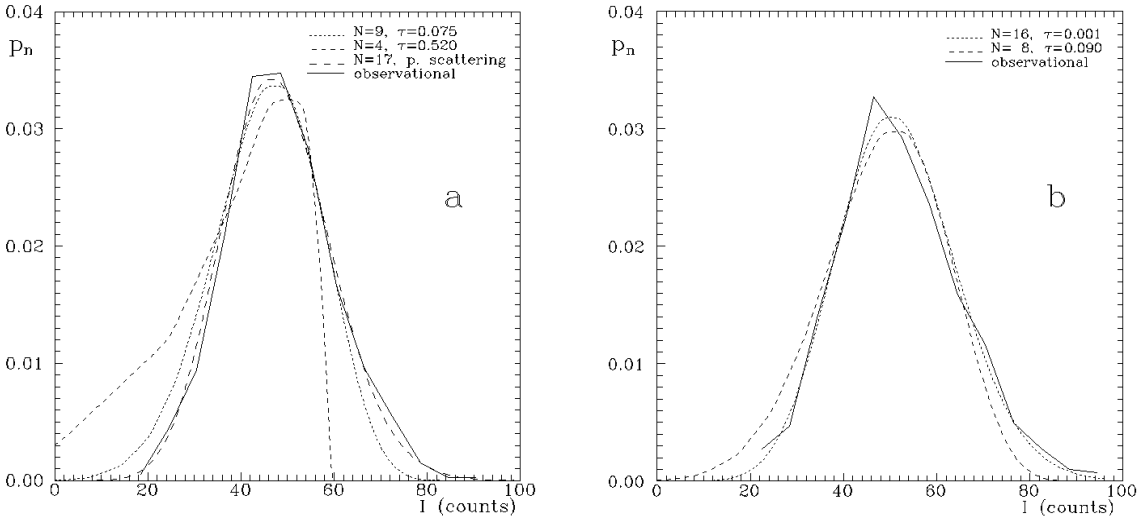

Fig. 6a and b. Theoretical and observational distributions of the line intensities (region nr. 2, Dec 18, 1973): **a** Ly-α line. The observational intensities show a nearly Gaussian probability distribution p_n. The theoretical ones are obtained involving the core-emission model. **b** CIII line. The observational intensities for the optically thin lines show an asymmetric probability distribution, p_n, tailed to greater intensities. The theoretical ones are constructed from the interface-emission model

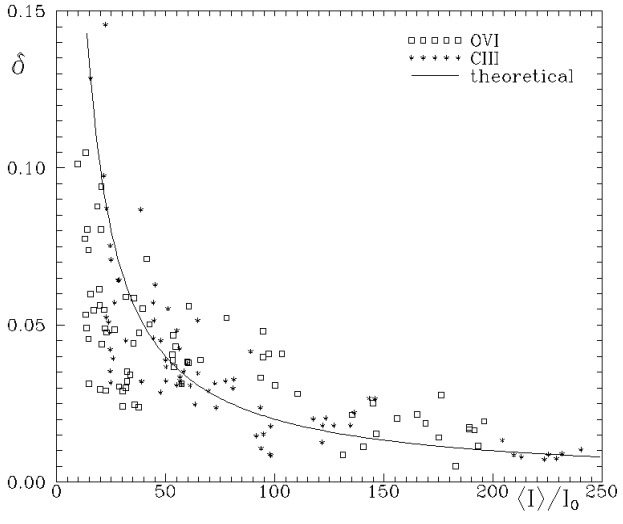

Fig. 7. The RelMSD, δ, depending on the mean intensity, $\langle I \rangle$, scaled by the initial energy released by a single layer, I_0. The points represent the values calculated from 9 different regions of the prominence observed on July 10 1973, in the CIII and OVI lines. The curve represents the theoretical expectation given by the interface-emission model with $\tau = 0$

presence of another fluctuation source, like physical inhomogeneities or the filling factor. The regions where these large δ values were measured generally correspond to prominence legs, where physical conditions may change radically.

We note that some differences occur between the observational values of δ for different optically thin lines, obtained in the same prominence region. In the optically thin case, our models predict fluctuations of almost the same level for all the lines. However, for some lines, initially presumed optically thin, absorption in the interface may become important, and thereby induce differences between RelMSD values. A theoretical model that takes into account absorption only through the interface has also been analysed but it is not presented here because its strong similarity to the core-emission model. For the concerned absorption range ($\tau \to 0$), the conclusion is that, supposing the same number of structures, different optical thicknesses induce rather small differences between the corresponding δ values. This result is valid for the slab, as well as for the thread model. Nevertheless, another difference occurs, and both mechanisms, absorption in the interface and in the core, can act together to yield the actual value of fluctuations. Note also that the emitting and absorbing envelope approach (and also the limit $\delta \cong 1/N$), applied to a given spectral line, does not depend on absorption in other layers, nor on emission in other lines than in the one concerned. Hence, this does not exclude the possible hypothesis of the existence of a different number of isothermal independent elements.

As might be expected, the Poisson distribution of components leads to satisfactory results for optically thin lines. The observed distributions of intensities in all the considered lines are highly asymmetric, tailed to greater intensities. Such an example is shown in Fig. 6b, for the distribution of the CIII line intensities. For a low absorption range, the distributions provided by the theoretical intensity exhibit an analogous asymmetry. Consequently, we see from Fig. 6b that the theoretical distributions with very small values of τ, and N between $5-20$ fit the distribution of the observed intensities with a high level of confidence. The pairs (N, τ) used in Fig. 6b were obtained from Eq. (21) for the observed value of δ.

We showed that the application of the interface-emission model for lines with either small or large absorption in the core

predicts, for the same N values, a smaller RelMSD for the latter. We see from Table 3 that this is not confirmed by observations. In fact, the OIV line which exhibits large absorption in the Lyman continuum in the cool central parts, shows larger values of relative variance, as compared to those beyond the Lyman limit. One possible explanation is that, for a great optical thickness, the thread model yields greater values of δ, if the emitting shell is large or distant from the absorbing centre. Another reason for this discrepancy could be the inaccuracy in the determination of the observed value of the RelMSD for the OIV line. The observed intensities in this line are very low, which induces a high noise to signal ratio, accounting for the large value of δ. The same effect could arise for the MgX and CII lines, that also exhibit small intensities and large fluctuations. Note that the geometrical models should be modified for the interpretation of intensity variations of the line MgX λ625Å, which is characteristic mainly for the coronal regions.

5.3. Number of structures

From the observational values of the mean intensity and RelMSD, we can estimate some important parameters of solar prominences. In particular, we show that the values of the RelMSD depend only on the mean number of structural elements in the line-of-sight and the optical thickness of the core. Generally, pairs of N and τ can be inferred from the observed values of δ, for both core and envelope emission. Another method to deduce the values of N and τ may be by comparing the theoretical and the observed distributions of intensity, which entails fitting the intensity distributions for various regions of the prominence.

First we consider the optically thick lines originating in the core of the structures. In this situation, the relationship $\delta\,(N, \tau)$ (core emission) is a very weak τ-dependent function, for large τ values. Its steep decrease with N enables us to estimate the expected number of elements along the line-of-sight. For example, for the Ly-α line, δ between 0.02, in the brightest regions, and 0.15 in the less intense ones, provide values of N between 4 and 2, respectively. As mentioned before, the pure scattering mechanism is more suitable for treating the Ly-α line, and gives for the mean number of elements, with the above values of the RelMSD, a value between 6 and 50. Fig. 6a, shows that a theoretical distribution with $N = 20$ approximates very well the observed distribution.

Next, we consider the case of the optically thin lines (CII λ1336Å, CIII λ977Å, OVI λ1032Å). It was shown in Sect. 3.2, that in the case when the central absorbing part of the structures becomes transparent ($\tau \rightarrow 0$) the interface-emission model gives $\delta \cong 1/N$. Therefore, a value of the RelMSD of $0.02 - 0.2$ gives for the mean number of features in the line-of-sight, $N = 5 - 50$. Assuming a thread geometry and the number of rows equal to 3, we obtain for the mean number of threads per pixel values between 15 and 150. If a small amount of absorption is taken into account, in either central parts or in the interface, this number decreases slightly, proportionally to the absorption. This can explain the differences between the RelMSD values of different spectral lines, obtained in the same prominence region. Alternatively, the shape of the interface could change at different temperature levels of the structures. In some cases, a single high temperature shell could surround several lower temperature features, implying that a smaller mean number of components should be obtained using lines formed in this shell. For example, slightly greater values of δ (and consequently smaller values of N) are obtained for the line OVI λ1032Å ($T = 3 \times 10^5$ K), as compared to those for the line CIII λ977Å ($T = 8 \times 10^4$ K). For very small values of the optical thickness, the fitting of the observed intensity distributions with the ones derived with the interface model gives N between 5 and 20.

In conclusion, the above results allow us to assume the existence of a relatively small number of structures in the line-of-sight. The same number of cool absorbing cores and hotter emitting envelopes is found, when either optically thick or optically thin lines are used, i.e. approximately 5 elements are found in the faintest and 50 in the brightest regions. These estimates are restricted to lines formed at temperatures ranging from 10^4 to 3×10^5 K, i.e. in the prominence and in the transition zone. The situation may change at somewhat higher temperatures in the corona, where, due to the different physical nature, the supposed models and also the number of components may differ. Our results are generally in good agreement with those obtained by other authors, see Sect. 1. Note that, even if the observed pixel had different dimensions, the result represents the mean number of structures integrated along the line-of-sight and does not depend on the geometrical model or on the filling factor. Moreover, for some bright regions, the number of components obtained approaches the much greater values ($50 - 200$), determined from the non-LTE modelling of hydrogen lines (Fontenla et al. 1996).

6. Conclusive remarks

In this paper we have studied the prominence spectrum by considering the transfer of radiation through randomly distributed fine structures. Two cases of the line formation were treated (core and interface emission). For each of them, two geometrical models were employed, slabs and threads. The main hypothesis was that the observed intensities and their fluctuations are due only to the random character of the number of structures in the line-of-sight, which is distributed according to Poisson's law. Consequently, we compared the theoretical and observational intensity distributions and their characteristics – mean intensity, relative variance (RelMSD) – in order to estimate the geometrical and physical parameters of the prominences.

We first conclude that, generally, the geometrical model is not of major importance for the degree of brightness fluctuations, so that other reasons must be considered in the interpretation. Therefore, when analysing the variations of intensity, a single geometry may be considered. The comparison of the theoretical values of the RelMSD with observed values shows that, generally, the models predict well the observational behaviour of this parameter. The theoretical distribution of intensities fits the observational distribution for most of the presented cases.

The results allow us to determine the existence of a relatively small number of structures in the line-of-sight.

Acknowledgements. This research was supported by the French Ministry of Foreign Affairs (S.P.) and by NATO under grant CRG 960346 (A.G.N.). The authors thank the Principal Investigator of the Harward experiment, Dr. Robert W. Noyes, and the National Space Science Data Center through the World Data Center A for Rockets and Satellites for the Skylab prominence observations. We are pleased to thank the referee, E. Tandberg-Hanssen, for careful reading of the manuscript and useful suggestions.

References

Engvold, O., 1976, Solar Phys. 49, 283
Engvold, O., Kjeldseth-Moe, O., Bartoe, J.-D.F., and Brueckner, G.E., 1987, in: 21st ESLAB Symp., Bolkesjø, Norway, June 22–25, ESA SP-275, 21
Engvold, O., Jensen, E., Zhang, Y., and Brynildsen, N., 1989, Hvar Obs. Bull. 13(1), 205
Fontenla, J.M., Rovira, M., Vial, J.-C., Gouttebroze, P., 1996, ApJ 466, 496
Nikoghossian, A.G., Pojoga, S., Mouradian, Z., 1997, A&A, 325, 813
Orrall, F.Q., Schmahl, E.J., 1980, ApJ 240, 908
Pojoga, S., Nikoghossian, A.G., Mouradian, Z., 1997, in: IAU Coll. 167, New Perspectives on Solar Prominences, Webb, D., Schmieder, B, Rust, D. (eds.), in press
Reeves, E.M., Huber, M.C.E., Timothy, J.G., 1977, Appl. Opt. 16, 837
Stellmacher, G., Wiehr, E., 1994, A&A 290, 655
Stuart, A., Ord, J.K., 1991, Kendall's Advanced Theory of Statistics, Edward Arnold, London
Tandberg-Hanssen, E., 1995, The Nature of Solar Prominences, Kluwer, Dordrecht
Vernazza, J.E., Foukal, P.V., Huber, M.C.E. et al., 1975, ApJ 199, L123
Zirker, J.B. and Koutchmy, S., 1990, Solar Phys. 127, 109

This article was processed by the author using Springer-Verlag LaTeX A&A style file *L-AA* version 3.